JOURNAL OF MATERIALS SCIENCE 15 (1980) 1147–1152

Intrinsic stress in thin films of Ag, Al, ZnS and LiF

M. LAUGIER*
Laboratoire d'electrotechnique, Université d'Aix-Marseille III, Centre de Saint-Jérôme, 13397 Marseille, France

The intrinsic force per unit width, S, in thin films of Ag, Al, ZnS and LiF prepared by vacuum evaporation at pressures of less than 5×10^{-5} Torr, has been investigated using a sensitive bending plate technique with capacitative detection. In each case the intrinsic force S was found to vary linearly with film thickness f, for thicknesses greater than about 100 Å, leading to a constant intrinsic stress $\sigma = dS/df$. Both S and σ were found to be compressive for ZnS and Al, and tensile for Ag and LiF.

1. Introduction

Intrinsic stress is related to the structure and growth of the film, and is that stress remaining after elastic stresses of thermal origin have been accounted for. High stress can lead to degradation of the film: dielectric films used for optical purposes may "cloud" if the stress leads to internal rupture; metal films which are generally under tension may "craze", and peeling is sometimes observed; films which are under compression may fail by buckling when the film–substrate adhesion is overcome.

Although the existence of residual film stress has long been known, it is only recently that semi-quantitative models for its origin and development have been proposed. There are three basic ways of determining film stress: by means of the induced deformation of a thin substrate, by lattice spacing measurements, or by measurement of some other stress-dependent property. These methods have been reviewed by several authors [1, 2]. The first method is the most direct, and the most sensitive, and consequently the majority of stress results have been obtained by this means.

In the present work, intrinsic stress in Ag, Al, ZnS and LiF is investigated from the early growth stages to thicknesses of about 1000 Å, using a sensitive cantilevered plate technique with capacitative detection.

2. Experimental details

2.1. Stress measuring apparatus

The cantilevered plate – the substrate – in the form of a glass cover slip was clamped rigidly along one edge to a simple jig using an Alnico bar magnet to form a parallel plate capacitor, as shown in Fig. 1. (The surface of the cover slip facing the jig was metallized.) The small capacitance changes caused by substrate bending during film deposition were monitored using a capacitance bridge (a Fielden Proximity Meter was found suitable). The Proximity Meter output was fed directly to a suitable chart recorder, and a calibration graph was drawn of chart reading versus change in capacitance in pF. The chart recorder sensitivity used was 0.1 V F.S.D. The Proximity Meter stability was excellent at all sensitivity settings as verified by setting up using a high quality calibrated variable air capacitor – a General Radio type 722 (GR 722) – no drift occurred

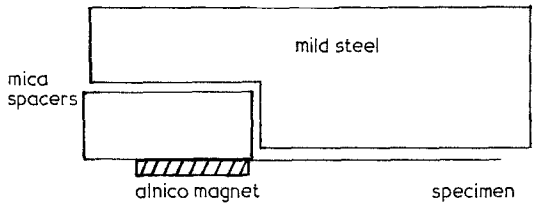

Figure 1 Specimen holder.

*Present address: Wimet Ltd, Research and Development Laboratories, Torrington Avenue, Coventry.

0022–2461/80/051147–06$02.60/0

over the observation periods which extended up to 6 h. The sensitivity as used in the experiments was of the order of 2×10^{-2} pF cm^{-1} on the chart recorder, and the output was linear with change in capacitance. This corresponded to an experimental sensitivity of close to 7 dyn cm^{-1}.

2.2. Mounting of the apparatus

Initially, operational stability was not good at high Proximity Meter sensitivities, even though the rotary pump was decoupled and connected to the vacuum unit only via a flexible rubber hose, and the unit itself was mounted on rubber bushings. The instability was traced to vibration being transmitted to the system via the flexible hose itself. This was effectively removed by making two flexible connections: one from the pump to a securely fixed metal junction-piece on a wall, and the other from this to the system.

The internal bell-jar connections were rigid, and the bell-jar was internally coated with Al, and earthed, to provide the necessary electrostatic screening.

The bridge was found to become unstable when operated under a glow discharge, and whenever charged particles were incident on the jig. The stability of the system under operation thus indicated that charges were not reaching the jig, i.e. that the depositing vapour was electrically neutral. This observation is of interest in connection with the electrostatic theory of film stress [3], in which charges are assumed to be present on the growing islands, leading to stress in the film.

2.3. Specimen selection

The specimens were selected Chance–Pilkington microscope cover slips $5 \times 2.2 \times 0.015$ cm^3. Selection was carried out by observing the interference fringes formed by reflection at both surfaces and viewed in transmission in monochromatic light from a mercury lamp. The cover slips were clamped along one edge for this purpose, to match the experimental conditions. Those cover slips that did not produce straight interference fringes were discarded.

2.4. Specimen preparation

The slides were scrubbed in "Teepol" and thoroughly rinsed in hot running water, then dried using lens tissue. This procedure was carried out just prior to use. The slides were then placed in position in the vacuum system, and a 200 Å layer of aluminium deposited. The system was then let up to atmospheric pressure, and the slide was correctly positioned in the jig with its metallized surface facing the jig reference surface.

At this stage, with the metallized cover slip clamped in position in the jig, a stress measuring experiment may be carried out.

2.5. Outgassing and deposition

The work was performed in a conventional Edwards type vacuum unit pumped by a silicon oil diffusion pump and backed by a rotary pump. Al was evaporated from tungsten spirals, Ag, ZnS and LiF were evaporated from Mo boats. The specimen was placed at about 20 cm from the vapour source. Prior to deposition, careful outgassing was performed, and a small amount of material was evaporated with a rotary shutter masking the specimen.

2.6. Glow discharge cleaning

Prior to evaporation, and when the pressure in the bell-jar had reached the 2 to 5×10^{-5} Torr range, air was leaked in through a needle valve and an a.c. glow discharge was set up; care was taken to ensure that the specimen was immersed in the plasma which provides efficient cleaning and not in a dark space, as it is well known that electron bombarment causes polymerization of the hydrocarbons present in the vacuum system emanating from the diffusion pump oil which then form a contaminationg layer on the specimen surface.

2.7. Thickness

Thickness measurements were made using an Edwards quartz crystal thickness monitor incorporating a rate meter attachment. Calibration was performed using Tolansky's method of multiple beam interferometry [4].

2.8. Thermal effects

Temperature measurements on identical cover slips positioned adjacent to the specimen using chromel–alumel thermocouples bonded to the face furthest from the vapour source using "silver paste", had indicated temperature rises during deposition of the order of 10° C. Thermal cycling of experimental substrates using radiant heat from an empty boat over this range had shown that substrate bending observed during the heating decayed to equilibrium within about 4 min.

2.9. Technique

Films were deposited sequentially, in layers of less than 200 Å, and bending force measurements were made after a standard time of 4 min had elapsed after deposition. By this means, thermal effects were minimized.

It was, in fact, the change in capacitance that was measured, and in order to relate this to the bending force S, the starting capacitance was required. This was measured by a substitution method making use of the standard capacitor GR 722, and was typically of the order of 18 pF.

2.10. The relation between substrate deformation and bending force

The relation between the internal bending force per unit width of film S, and the bending induced in the substrate, was first given by Stoney [5] as:

$$S = E_s \frac{t^2}{6r}, \tag{1}$$

where E_s is the substrate Young's modulus, t is the substrate thickness and r is the substrate radius of curvature. More detailed calculations have been made by several authors [6, 7], but for beam geometry, they reduce to Equation 1 as long as the thickness of the deposit and the displacement of the free end are both small compared with the thickness of the beam.

In the present experiments, plate geometry was used and in this case the lateral substrate contraction must be taken into account. Equation 1 is then modified to [7]

$$S = \frac{E_s}{1-\nu} \cdot \frac{t^2}{6r} \tag{2}$$

where ν is the Poisson's ratio of the substrate.

2.11. The relation between capacitance change and bending force

In order to apply the modified Stoney formula, Equation 2, it is necessary to derive a relation between r the radius of curvature of the substrate, and ΔC the change in capacitance between the reference surface and the specimen. Fig. 2 is used for the calculation.

If y_0 is the original parallel plate capacitor spacing before bending, and if $y(x)$ represents the equation of the curved specimen, then the total capacitance between the specimen and the reference surface after bending is

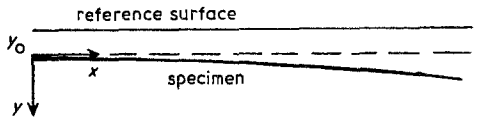

Figure 2 Notation used for calculation of the relation between capacitance change and bending force.

$$C = \int_0^l \frac{\epsilon_0 b}{y_0 + y} \mathrm{d}x \text{ Farad} \tag{3}$$

where l is the specimen length, b its width and $\epsilon_0 b \Delta x/(y_0 + y)$ is the capacitance of a section of the system of length Δx. When the displacement of the free end is small, the following expression may be used for the radius of curvature r, of the cantilever: $r = x^2/2y$, where (x, y) refers to a point on the specimen surface.

Substituting for y in Equation 3 and integrating gives:

$$C = \frac{\epsilon_0 lb}{y_0} \cdot (2ry_0)^{\frac{1}{2}} \tan^{-1} \frac{l}{(2ry_0)^{\frac{1}{2}}}. \tag{4}$$

The following formula is obtained by retaining only the first two non-vanishing terms of a Taylor expansion of Equation 4:

$$C = C_0 - \frac{\epsilon_0 lb}{y_0^2} \cdot \frac{l^2}{6r}$$

where the initial capacitance

$$C_0 = \frac{\epsilon_0 lb}{y_0}. \tag{5}$$

The formula of Equation 5 is accurate within the limitations of beam theory: a limiting free end displacement of $y_{max} = t$, the substrate thickness, would require the large bending force $S \sim 150 \times 10^3$ dyn cm^{-1} (in this work $S_{max} \sim 8 \times 10^3$ dyn cm^{-1}), and in the present experimental arrangement this would only lead to a 1% error over the correct result of Equation 4. Using Equation 4, an expression accurate to within 0.05% may be written for the capacitance change due to bending of the specimen to a radius of curvature r:

$$|C - C_0| = \Delta C = \frac{C_0^2}{\epsilon_0 lb} \cdot \frac{l^2}{6r}. \tag{6}$$

Combining Equation 6 with the modified Stoney formula, Equation 2, gives the relation between the bending force S and change in capacitance ΔC as:

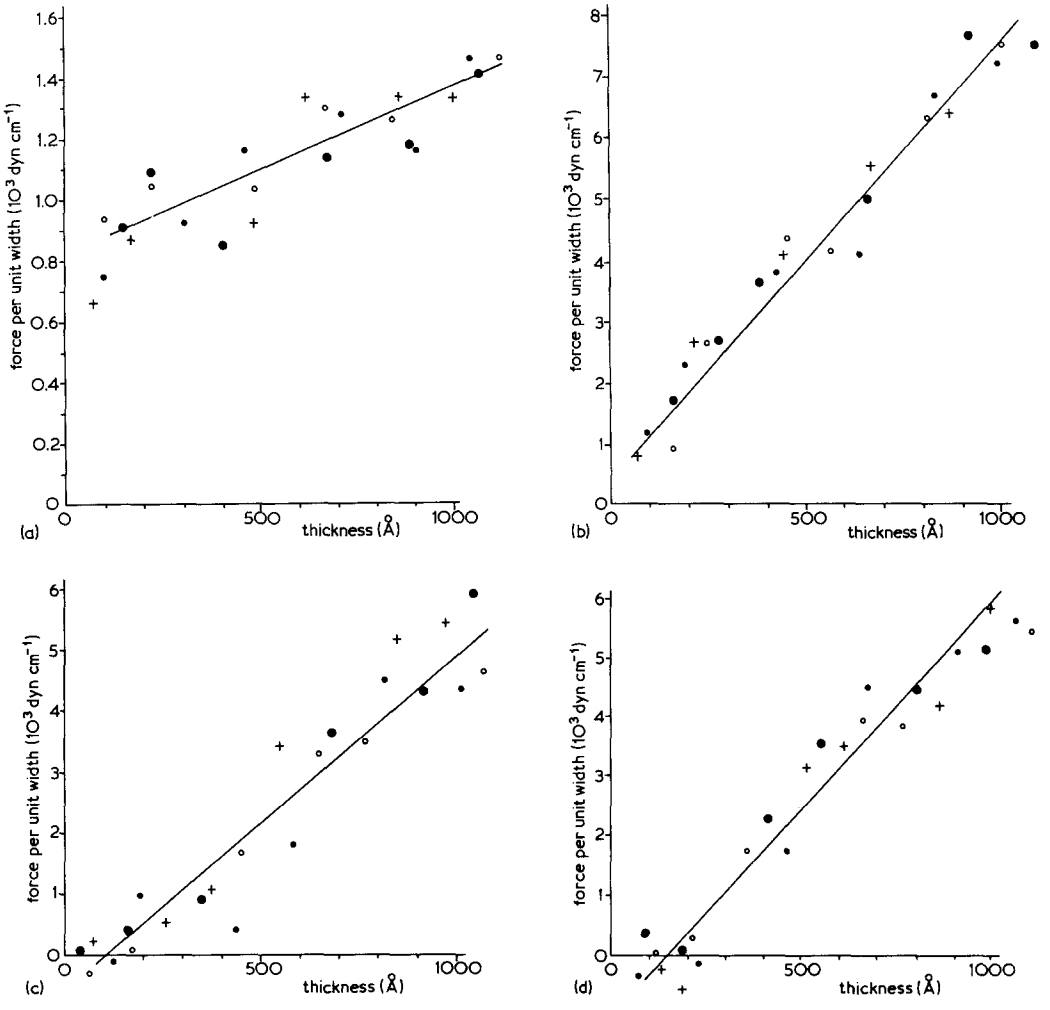

Figure 3 Intrinsic bending force versus thickness for films of Ag, Al, ZnS and LiF. Each type of point refers to a separate experiment for each material. (a) Results for the tensile intrinsic force in Ag. Rate of deposition 10 Å sec^{-1}. (b) Results for the compressive intrinsic force in Al. Rate of deposition 5 Å sec^{-1}. (c) Results for the compressive intrinsic force in ZnS. Rate of deposition 5 Å sec^{-1}. (d) Results for the tensile intrinsic force in LiF. Rate of deposition 10 Å sec^{-1}.

$$S = \frac{E_s}{1-\nu} \cdot \left(\frac{t}{l}\right)^2 \cdot \frac{\Delta C}{C_0^2} \cdot \epsilon_0 lb$$

which is the relation required. The symbols have the usual meaning.

3. Results

Data obtained in four separate experiments on each material are shown plotted in the form bending force per unit width versus film thickness in Fig. 3 a to d. The thickness range investigated was from about 50 to 1000 Å.

The results for a given film did not lie on a smooth curve, though when the results for four different films prepared under the same conditions of pressure and rate of deposition were plotted together, a clear general trend could be seen and lines have been drawn to indicate this.

In each case a linear bending force S versus thickness relation was found for films thicker than about 100 Å, corresponding to a constant intrinsic stress σ over the range about 100 to 1000 Å. Both S and σ were found to be compressive, (the film would "like" to expand) for ZnS and Al, the tensile (the film would "like" to contract) for Ag and LiF.

In summary, therefore, intrinsic stress in Al deposited at 5 Å sec^{-1} was found to be compressive and its value was about 7.4×10^8 dyn cm^{-2}, that in Ag deposited at 10 Å sec^{-1} was tensile and

its value was about 0.7×10^8 dyn cm^{-2}. The intrinisic stress in ZnS deposited at 5 Å sec^{-1} was compressive and its value was about 6.3×10^8 dyn cm^{-2}, and in LiF deposited at 10 Å sec^{-1} was tensile and its value was about 7.1×10^8 dyn cm^{-2}.

4. Discussion

A detailed investigation of the earliest stages of growth was not made in this work, but the tendencies that are indicated for film thicknesses below ~ 100 Å were confirmed by later work which employed a new bending plate technique [8] and which will be the subject of a subsequent article.

The bending force S found in Ag was similar in magnitude to that reported by other workers [9–11]. The small constant stress, $\sigma = \mathrm{d}S/\mathrm{d}f$, found in Ag beyond the early growth stages, confirms results of Maki *et al.* [9], but contrasts with the compressive and zero stresses that have also been reported [9–11].

The constant compressive stress found in Al, although agreeing with Murbach and Wilman's results [12] obtained under similar conditions, is nonetheless unusual. Al has been studied [13–15] using a variety of substrate materials (but not glass) and has been found to develop a tensile stress, characteristic of pure structures.

The results found for LiF are in close agreement with those of other workers [16, 17]. However, the initially compressive bending force has not been previously reported.

The slight initial tension observed in ZnS confirms recent observations of this effect [12, 18], and the region of constant compressive stress is also in general agreement with results of other workers [12, 18, 19]. Detailed comparisons are made difficult as the experiments were performed under different conditions.

The following current models would seem to offer a qualitative explanation of the results.

4.1. Surface disorder model [20]

It is claimed that the tensile stresses observed in many metals are due to the rearrangement and constrained shrinkage of disordered material buried under the advancing surface of the growing film. It is considered that arriving atoms can move about on the surface to improve the crystalline order, but would be frozen when they were buried. Rearrangement would occur later at a slower rate resulting in shrinkage. Assuming annealing on the surface to be a thermally activated process, it was deduced that for deposition rates of the order of a few angstroms per second, that a high or a low stress would be developed if $T_m/T_s > 4.5$ or $T_m/T_s < 4.5$ respectively. T_m is the melting point and T_s the substrate temperature. This reasoning was confirmed in experiments on nickel films [21].

This model leads to a constant tensile stress, and would therefore provide a qualitative explanation for the small constant tensile stress found in Ag, which satisfies the requirement $T_m/T_s < 4.5$. The model does not seem to apply to LiF, which develops a large constant tensile stress, although $T_m/T_s < 4.5$.

4.2. Grain-boundary relaxation model [22–24]

In this model, the interatomic forces acting across the gap between two grains as they grow together, are considered to cause an elastic relaxation of the grain walls, leading to tension in the grains which at this stage would be constrained to the substrate. If the grains recrystallized to form larger ones during growth, a three-dimensional rearrangement of the atoms during this process would eliminate the strains produced by the former grain boundaries. Thus the film stress would be determined by the forces acting at the boundaries of the final grains. The model has had some success in the case of nickel films, but the grain wall relaxation is sensitive to the form chosen for the interatomic force potential.

This model leads to a tensile intrinsic stress which is inversely proportional to the grain diameter in continuous films. The model could account for the constant tensile intrinsic stress in Ag and LiF beyond the early growth stages if the grain diameter in the plane of the film remains constant.

4.3. Grain growth model [25]

This model is based on the elimination of grain boundaries during growth, which is assumed to occur without relaxation of strain during recrystallization. The following formula for the intrinsic bending force S may be derived from the above assumptions:

$$S = \left\{ \frac{E_f}{1-\nu_f} \alpha a \left(\frac{1}{\langle D_0 \rangle} - \frac{1}{\langle D \rangle} \right) + \bar{\sigma}_0 \right\} f,$$

where S is the force per unit width, E_f is Young's modulus for the film, ν_f is Poisson's ratio for the

film, a is the normal atomic distance and α is a constant which gives the average grain-boundary width as $(1 + \alpha)a$. $\langle D \rangle$ and $\langle D_0 \rangle$ are the average grain diameters at thicknesses d and d_0 and $\bar{\sigma}_0$ is the average film stress observed at thickness d_0.

This model has been employed to discuss stress results in continuous films of Ag, Au and Cu deposited onto mica substrates [26], which showed a linear bending force versus film thickness relation, on the basis that $d/\langle D \rangle = d_0/\langle D_0 \rangle$. It may be noted that the model can only give a linear intrinsic force S versus thickness relation when $\langle D \rangle \propto d$. On this basis, the model could account for the constant tension σ observed in continuous films of Ag and LiF.

4.4. Impurities model

Impurities generally lead to compressive stresses. It has been estimated [27] that 1 at % oxygen impurity incorporated into the film during growth in films of Ni leads to a compression of 4×10^9 dyn cm^{-2}. On this basis, the compression observed in Al would be explained by the incorporation of only 0.18 at % oxygen. This is not unlikely, as it has been found by Auger spectroscopy that films of Ti–Cr prepared by electron beam evaporation at pressures between 5×10^{-7} and 5×10^{-8} Torr, contain between 0.6 and 0.8 at % oxygen [28].

In a similar fashion, the constant compressive stress observed in ZnS beyond the early growth stages might be attributed to small quantities of Zn or S or their oxides incorporated in the ZnS film during growth, as ZnS is known to dissociate slightly on evaporation.

5. Conclusion

A sensitive cantilevered plate method of intrinsic stress determination using capacitative detection has been described. Results have been obtained for intrinsic stress in thin films of Ag, Al, LiF and ZnS, and in each case a linear bending force versus film thickness relation was found for films beyond the early growth stages. The results obtained have been discussed in terms of several current models.

References

1. R. W. HOFFMAN, in "Physics in Thin Films 3" (Academic Press, 1966).
2. D. S. CAMPBELL, "Handbook of Thin Film Technology", edited by L. I. Maissel and R. Glang (McGraw Hill, 1969).
3. D. B. DOVE, *J. Appl. Phys.* 35 (1964) 2785.
4. S. TOLANSKY, "Multiple Beam Interferometry" (Clarendon Press, Oxford, 1948).
5. G. G. STONEY, *Proc. Roy. Soc. A* 32 (1909) 172.
6. A. BRENNER and S. SENDEROFF, *J. Res. Nat. Bur. Stand.* 42 (1949) 105.
7. N. N. DAVIDENKOV, *Sov. Phys. Sol. State.* 2 (1961) 2595.
8. M. T. LAUGIER, *Thin Solid Films* 66 (1980), to be published.
9. K. MAKI, Y. NAKAJIMA and K. KINOSITA, *J. Vac. Sci. Technol.* 6 (1969) 622.
10. K. KINOSITA, H. KONDO and I. SAWAMURA, *J. Phys. Soc. Japan* 15 (1960) 942.
11. J. D. WILCOCK, D. S. CAMPBELL and J. C. ANDERSON, *Thin Solid Films* 3 (1969) 13.
12. A. E. ENNOS, *Appl. Opt.* 5 (1966) 51.
13. H. P. MURBACH and H. WILMAN, *Proc. Phys. Soc. London* B66 (1953) 905.
14. T. B. RYMER, *Proc. Roy. Soc. London* A225 (1956) 274.
15. E. KLOKHOLM, *J. Vac. Sci. Technol.* 6 (1969) 138.
16. H. BLACKBURN and D. S. CAMPBELL, *Phil. Mag* 8 (1963) 823.
17. R. CARPENTER and D. S. CAMPBELL, *J. Mater. Sci.* 2 (1967) 173.
18. R. J. SCHEUERMAN, *J. Vac. Sci. Technol.* 7 (1970) 143.
19. H. BLACKBURN and D. S. CAMPBELL, *Trans. 8th. Nat. Vac. Symp.* (1961).
20. E. KLOCKHOLM and B. S. BERRY, *J. Electrochem. Soc.* 115 (1968) 823.
21. E. KLOCKHOLM, *J. Vac. Sci. Technol.* 6 (1969) 138.
22. F. A. DOLJACK and R. W. HOFFMAN, *Thin Solid Films* 12 (1972) 71.
23. R. W. SPRINGER and R. W. HOFFMAN, *J. Vac. Sci. Technol.* 10 (1973) 238.
24. R. W. HOFFMAN, *Thin Solid Films* 34 (1976) 185.
25. P. CHAUDHARI, *J. Vac. Sci. Technol.* 9 (1972) 520.
26. Y. NAKAJIMA and K. KINOSITA, Proceedings of the 6th International Vacuum Congress (1974) in *Jap. J. Appl. Phys. Suppl. 2, Part 1* (1974) 575.
27. P. M. ALEXANDER and R. W. HOFFMAN, *J. Vac. Sci. Technol.* 13 (1976) 96.
28. H. C. TONG, C. M. LO and W. F. TRABOR, *ibid* 13 (1976) 99.

Received 12 July and accepted 13 September 1979.